Relationship of phase diagrams and surfaces of new phase nucleation rates

M. P. Anisimov, P. K. Hopke, D. H. Rasmussen, S. D. Shandakov, and V. A. Pinaev

Citation: The Journal of Chemical Physics **109**, 1435 (1998); doi: 10.1063/1.476694
View online: http://dx.doi.org/10.1063/1.476694
View Table of Contents: http://scitation.aip.org/content/aip/journal/jcp/109/4?ver=pdfcov
Published by the AIP Publishing

Relationship of phase diagrams and surfaces of new phase nucleation rates

M. P. Anisimov and P. K. Hopke
Department of Chemistry, Clarkson University, Potsdam, New York 13699-5810

D. H. Rasmussen
Department of Chemical Engineering, Clarkson University, Potsdam, New York 13699

S. D. Shandakov and V. A. Pinaev
Kemerovo State University, 6 Krasnaja Street, 650099, Kemerovo, Russia

(Received 5 September 1997; accepted 17 April 1998)

Experimental and theoretical investigations of vapor nucleation began about 100 years ago. Until the 1980s, experiments generally measured only critical supersaturation values. Since then, measurement procedures have substantially improved and nucleation rates can now be measured as a function of temperature, vapor activities, and pressure with high accuracy. Nucleation theory has made obvious progress, but the understanding of nucleation phenomenon is far from complete. New approaches to conceptualizing nucleation are necessary in order to identify possible new directions for further improvement of nucleation theory. One such approach is the analysis of the topology of nucleation rate surfaces. The creation of a nucleation rate surface is based on knowledge of phase equilibrium diagrams, limited experimental nucleation results, and a few plausible assumptions. In this article, the surfaces of the nucleation rates as a function of pressure or activity for single and binary systems for nucleation from metastable vapor, liquid, and crystalline states are constructed. By using surface topology analysis, some problems in nucleation theory are more clearly formulated and future directions for improvement can be found. Currently, it is not possible to create a universal nucleation theory based only on first principles. Partial theoretical success can be obtained only in the case of systems with well-known molecular interaction potentials. By scaling the experimental nucleation rate surfaces for portions of the phase diagrams that are identical to one another, a semiempirical nucleation rate surface for an unknown system can be created from its phase diagram. Scaling should give quantitative nucleation rates. Phase diagrams must be more fully incorporated into the interpretation of experimental nucleation results and nucleation theory development. [S0021-9606(98)01728-0]

I. INTRODUCTION

Experimental investigation of vapor nucleation began about 100 years ago in 1897 with Wilson's invention of the piston cloud chamber.[1] At the same time, Gibbs[2] made the initial theoretical description of the new phase critical embryo. Farkas,[3] Becker–Doring,[4] Volmer–Weber,[5] Flood,[6] Frenkel,[7] and Zeldovich[8] subsequently developed a more complete nucleation theory, now termed ''classical nucleation theory.'' In 1950, Reiss[9] generalized this theory to interpret the nucleation of binary systems. Reiss introduced a new type of Gibbs energy surface, and an investigation of its surface features has enabled the solution of the differential equation that determines the kinetics of the nucleation process to be simplified. Since then, nucleation theory has made obvious progress, but the understanding of nucleation phenomenon is far from complete. New ideas are necessary for analysis of the possible directions to improve the nucleation theory. Such ideas can be found by analyzing the topology of nucleation rate surfaces.

The visualization of the statistical and dynamic properties of molecular systems as geometrical figures was initiated in Gibbs time when a diagram of phase states was named geometrical thermodynamics. Anisimov[10] first reported the topology of the nucleation rate surface over a pressure-temperature (P-T) phase diagram with a triple point in 1990. The initial evaluation of the topology of a binary vapor nucleation surface was presented in 1994.[11] In this article, nucleation rate surfaces will be constructed for single and for binary system nucleation from metastable vapor, liquid, and crystalline states.

II. CLASSICAL NUCLEATION THEORY

Classical nucleation theory assumes that each embryo is able to grow or shrink by the gain or loss of single molecules. When clusters grow by adding single molecules A_1, the derivative of concentration $C(n)$ of n-size clusters with respect to the time, t, can be written in a discrete form:

$$\frac{\partial C(n)}{\partial t} = J(n+1,t) - J(n,t), \tag{1}$$

where $J(n+1,t)$ is the number of clusters changing from n to $n+1$ per unit time. If one neglects the discrete nature of the molecular events, embryo diffusion along the size axis can be written in differential form:

$$\frac{\partial C(n,t)}{\partial t} = -\frac{\partial J(n,t)}{\partial n}, \tag{2}$$

$$J(n,t) = \beta_n N c(n,t)\ \frac{\partial}{\partial n}\frac{C(n,t)}{c(n,t)}, \tag{3}$$

where $c(n,t)$ is an equilibrium concentration of size-n embryos at the time t. For steady state nucleation, $C(n,t) = C(n)$, $c(n,t) = c(n)$, $J(n,t) = J(n)$. Shneidman's[12] solution to these differential equations can be written in the following form:

$$C(n) = \frac{1}{2}\, c(n)\mathrm{erfc}\left(\frac{n-n^*}{\Delta}\right), \tag{4}$$

$$J = \frac{\beta_n N c(n^*)}{\Delta\sqrt{\pi}}, \tag{5}$$

$$\Delta = \left(-\frac{1}{2kT}\frac{\partial^2 \Delta G^*}{\partial n^2}\right)^{-1/2}, \tag{6}$$

where Δ is the width of the saddle point, n^* is the number of molecules in a critical embryo, $c(n^*) = N\ \exp[-\Delta G^*/kT]$, ΔG^* is the Gibbs free energy of formation of a critical embryo of a new phase from monomer in the supersaturated phase, k is the Boltzmann constant, and T is the absolute temperature. J is the number of clusters crossing the free-energy barrier, i.e., becoming capable of growth, per unit volume per unit time, i.e., the vapor nucleation rate. The discreet form of the above differential equations permits the use of a relatively simple computer simulation of the embryo diffusion along the size axis. Such computer experiments, though popular, require estimating the behavior of the accommodation coefficients.

The classical theory of nucleation uses a single cluster as the model of a unit with the average physical parameters for a cluster ensemble. In a real nucleating system, the critical embryo of a new phase contains from several molecules (atoms) to several hundred molecules (atoms). This quantity is too small to be described in thermodynamics terms. Hill[13] has shown that it is possible to use thermodynamics to describe small clusters as a statistical ensemble. In the original classical form a rate of nucleation is expressed by

$$J = Z\beta_n N_1\ \exp\left(-\frac{\Delta G^*}{kT}\right), \tag{7}$$

where Z is the Zeldovich nonequilibrium factor. It expresses the deviation of the actual concentration of the critical embryos from an ''equilibrium'' value. The kinetic factor, $\beta_n = 4\pi r^{*2} p_v [2\pi m kT]^{-1/2}$, is the impingement frequency of vapor molecules on the embryo surface. Here m is the molecular mass and $N_1 = p_v/kT$. The critical embryo Gibbs free energy ΔG^* can be calculated as

$$\Delta G^* = \frac{16\pi\sigma^3 \nu_l^2}{3(kT\ln S)^2}, \tag{8}$$

where σ is surface tension, v_l is a volume per molecule in a liquid phase, and S is vapor supersaturation ratio. The classical theory allows the calculation of the nucleation rate by using macroscopic values for the surface tension of the critical nucleus. Using macroscopic values for microscopic clusters is questionable. Because of this and other problems with classical theory, there have been efforts to develop alternative expressions for experimental nucleation rates, e.g., Girshick *et al.*,[14] Dilman–Meier,[15] and others.

In binary nucleation theory, the rate of homogeneous nucleation is predicted by an equation like that of Flood,[6]

$$J = B\ \exp[-\Delta G^*/(kT)], \tag{9}$$

where B is a kinetic factor and ΔG^* is the Gibbs free energy of a critical embryo of the new binary phase. The pre-exponential factor, B, was developed by Reiss,[9] Stauffer,[16] Mirabel and Katz,[17] and others.

Kassner and Schmitt[18] published a comparison of different theories and experimental results prior to 1966. At that time, the discrepancy between experimental and theoretical nucleation rates was due to low experimental reliability. Experiments, until the 1980s, generally measured only critical supersaturation. Measurement procedures have improved substantially and nucleation rates are now being measured as a function of temperatures, vapor activities, and pressures with high accuracy. Oxtoby[19] has reviewed contemporary theoretical and experimental advances in the study of homogeneous nucleation. The discrepancy between nucleation theory and the experimental results can be several orders of magnitude. This discrepancy indicates that the theory still has omitted important details in the description of the nucleation phenomenon.

III. SOME SURFACE TOPOLOGIES FOR FORMATION RATE OF NEW PHASES

A. The chemical potential surface

The chemical potential surface of a uniform phase as a function of the system temperature and the total pressure can be crossed by a chemical potential surface of another phase (Fig. 1). The intersection of the two surfaces is the interface equilibrium line. If the surfaces' first derivatives have a discontinuity along the line, a first order phase transition takes place. For the vapor-liquid equilibrium system shown in Fig. 1, the intersection line is the locus of points for phase transitions of the first order with a phase transition temperature, T_{pt}. The end of the line is the point of a phase transition of second order at the temperature T_c. The chemical potentials of the vapor and liquid phases and their first derivatives coincide at this point. A single phase is not sensitive to the interface equilibrium line. The phase can pass through it and reach the region where that phase's chemical potential is higher than the chemical potential of the other phase. These higher potential states are metastable, and are marked V_m and L_m in Fig. 1 for the vapor and the liquid states, respectively. The boundaries of the metastable states are the lines of the spinodal decomposition. In Fig. 1, the lines of the spinodal decomposition have projections cs_1 and cs_2 on the P-T plane. The projection of the intersection line generates the vapor-liquid equilibrium line, $T_{\mathrm{pt}}c$. In the case of a multicomponent system, there would be surfaces of multidimensional phase equilibrium, chemical potentials, and spinodal decomposition conditions.

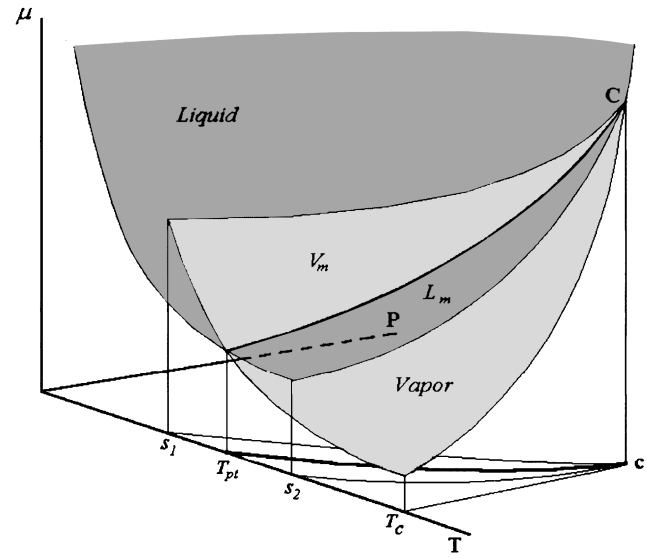

FIG. 1. The chemical potential, μ, for the vapor-liquid equilibrium as function of the system pressure, P, and temperature, T.

B. A simplified *P-T* diagram of metastable states

Metastable states arise in phase transitions of the first order because energy is needed to create the interface of the critical embryos. The lifetime of a metastable phase depends on the depth of penetration into the region of the other coexistent stable phase, that is, on the extent of supersaturation of the metastable phase. Metastable state diagrams for fusion and cavitation have been presented by Skripov and Faizulin.[20] The metastable vapor state diagram and the surface of vapor nucleation rates was discussed by Anisimov.[10] Recently, Debenedetti[21] published a critical review of the metastable states of liquids and solids.

The metastable states for a single component P-T phase diagram with one triple point are discussed here because of the relative simplicity of this system. Even so, the conceptual framework for developing the topology of nucleation rate surfaces can be demonstrated. Construction of the surfaces of the nucleation rates for more complicated phase diagrams is possible using the same basic framework as for this simple system. The applicability of this process to binary systems will also be demonstrated.

In Fig. 2, the regions of metastable states that exist for each phase are shown. Arrows represent the low temperature limit. The liquid, solid, and vapor states are marked by the letters L, S, and V, respectively. The subscript m denotes a metastable state.

1. Solid-liquid and liquid-solid transitions

The equilibrium phase lines do not always end at the triple point (for example, see Skripov and Baidakov[22]). Thus, the S-L equilibrium line can be continued through the triple point, t_p, to point b. At this locus, the S-L line has a point of intersection with the spinodal decomposition line kbd of the superheated or supertensioned crystal and with the spinodal decomposition line cbl of the supertensioned or supercooled liquid.

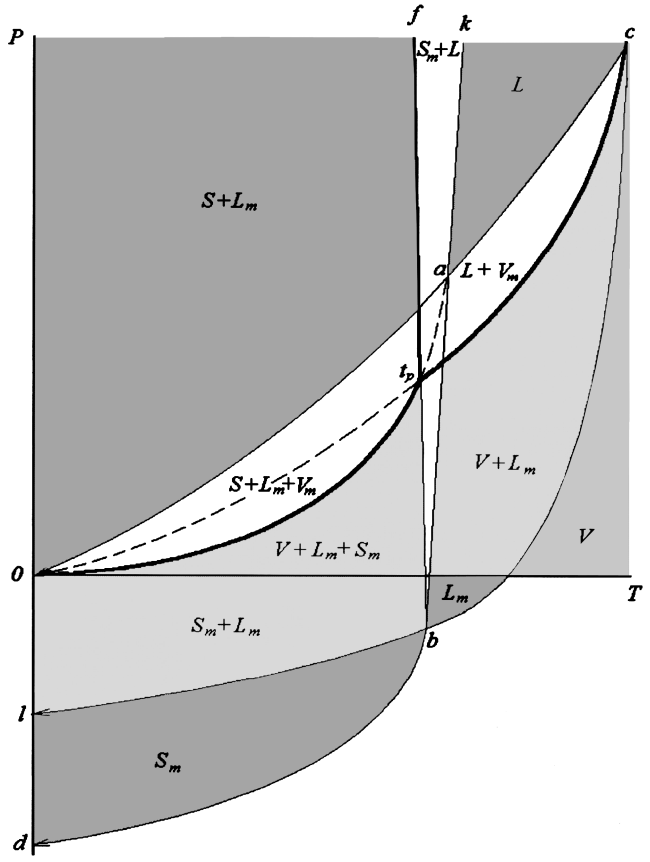

FIG. 2. A simplified P-T diagram of metastable states. The liquid, solid, and vapor states are marked by the letters L, S, and V, respectively. The subscript m denotes a metastable state; t_p—triple point; c—critical point; a and b—metastable critical points; arrows represent the absolute zero temperature limit.

Skripov and Faizulin[20] suggest that liquid states do not have limits down to absolute zero while others have argued for a liquid to crystal or liquid to other phase spinodal. If the liquid spinodal line exists, as discussed in the literature,[21,23] the surface topology of the supercooled liquid nucleation rate can be easily changed. These details are not pertinent to the current discussion of the general concepts for the construction of nucleation rate surfaces. Debenedetti[21] reviews the literature on liquid spinodal line conjecture and a possible second critical point for undercooled water. The models give a liquid to solid and/or a liquid tc vapor spinodal with and without second critical points. It is not the purpose of this paper to dwell on these issues. According to Rasmussen,[23] point b (Fig. 2) is a point of critical instability where the S-L equilibrium line intersects the cavitation spinodal lines cbl. At point b, the liquid state merges with the crystalline state in properties and structure just as the liquid and vapor state merge at the critical point c. However, at this point of critical instability, the now merged condensed states are also spinodally unstable to vaporization. It should be noted that there are other suggested phase state diagrams for spinodal line behavior in supercooled systems such as that of Speedy.[24] For the purposes of this paper, the differences between these spinodal lines will not be discussed as the issue is not what the phase diagram looks like but how a nucle-

ation rate surface can be constructed from a given phase diagram. The details of the nucleation rate surface for the liquid to solid and from solid to solid transitions will be reserved for a future effort.

The metastable vapor transitions to solid or liquid. The S-V equilibrium line extends from point a to point 0. It is reasonable to assert that the solid-vapor (S-V) equilibrium line begins at point a, where an intersection exists between the crystalline to liquid spinodal line kb and the vapor to liquid spinodal line $c0$. Point a is the highest temperature and pressure at which the (metastable) equilibrium solid-vapor exists because at infinitesimally higher temperatures, the crystalline state spinodally decomposes to liquid and at infinitesimally higher pressures, the equilibrium vapor spinodally decomposes to liquid. Point a is not a classical critical point like point c because, while both phases at point a are at the same temperature and pressure, they are still very different in density, structure and other properties, and, they are not spinodally unstable to decompose into each other but into a third phase, the liquid state. Thus, point a can be labeled a critical end point to the solid-vapor equilibrium curve but not a true critical point. The low temperature limit to the stability of the vapor state must approach zero pressure at absolute zero temperature.

2. Spinodals for vapor-crystalline and vapor-amorphous transitions

Amorphous states exist at low temperatures because of a kinetic limitation on the transformation to the more stable crystalline phases. It is plausible because of the lower mobility of molecules or atoms on the new phase embryo surface for the supercooled condition. As a result, the nucleation rate of the less ordered (amorphous) phase from the vapor is expected to be higher than that of the more ordered (crystalline) phase. If the nucleation rate of the crystalline phase were always larger than the nucleation rate of the amorphous phase, the amorphous state would not be observable, and this contradicts experimental experience. Glassy states of rapidly cooled liquids and vapor deposits are very well known. In aerosol production methods, the common experience is that one can obtain crystalline particles at relatively low supersaturations; even at pressures below the extrapolated equilibrium vapor pressure of the bulk liquid state. Only at sufficiently higher supersaturation can noncrystalline structured particles or supercooled liquid (or amorphous states) appear. The boundary lines for the onset of metastable vapor-liquid nucleation must be higher than the same boundary lines for vapor-crystal nucleation. On the other hand, instability of the vapor at the vapor spinodal boundary to condensation does not depend on the state to which the vapor will decompose and spinodal decomposition will provide fluctuations within which nucleation of any and all possible condensable phases depend upon the kinetics of the phase growth. Since the driving force for nucleation is highest and the critical nucleus size is smallest for all possible phase nuclei at the spinodal boundary, it is reasonable to argue that the maximum nucleation rate (irrespective of any phenomena like Ostwald ripening) of every phase will be observed at the spinodal boundary for the vapor. To identify the different surfaces of nucleation rates from the equilibrium boundaries of the bulk phases to the vapor spinodal, it is necessary to identify the phase of each nucleated particle. This level of detail is a problem for future studies.

C. Surfaces of nucleation rate superposed on the simplified *P-T* diagram

The surface of the nucleation rate can be constructed over a simplified P-T diagram with a triple point such as in Fig. 2. The surface will be discussed only in terms of steady state nucleation rates. Non-steady-state nucleation caused by limits on the mass and heat transfer processes, such as the time lag to establish stationary nucleation rates or vapor depletion effects, will not be discussed. To design a surface of the nucleation rate, the following rules were employed:

(1) A single phase can exist beyond its interface equilibrium lines. An interface equilibrium line can exist in an area of the other phase equilibrium state.
(2) The state diagram lines for the interface equilibria are the lines of the zero nucleation rate of the new phase embryos formation.
(3) The spinodal decomposition produces the highest nucleation rate for a given phase at a constant pressure or temperature.
(4) The nucleation rate for disordered and less stable states will be larger at the spinodal boundary than the nucleation rate of more ordered stable equilibrium states.
(5) A nucleation rate of new phase formation is equal to zero at the critical point.

The first three rules are the well-known empirical results for phase transitions of the first order. The fourth rule reflects the possibility that kinetic limitations can reverse the order of two different phase transitions. The fifth rule is the corollary of the second one. The second rule asserts that the equilibrium line is the locus of zero nucleation rate points. The critical point belongs to the equilibrium line and it has a nucleation rate of zero. This result is in agreement with classical theory.

To illustrate these rules, the surface of liquid cavitation (or boiling) rate, J, over the P-T phase diagram is shown in Fig. 3. Line cl is a spinodal as suggested by Skripov and Faizulin.[20] The spinodal line is the projection of the highest nucleation rate line, hc. This line has a finite (nonzero) low temperature limit and a zero rate of nucleation at the critical point. The crystalline-vapor equilibrium is shown by the dotted line t_p0.

The rate surface is drawn between the equilibrium line, ct_p0, the zero rate line, and the line ch. At the low temperature limit, the amorphous state (metastable liquid) degrees of freedom are reduced, and an accommodation probability of a single molecule on the cluster increases with decreasing temperature. Because of this, the surface has an absolute zero temperature limit nucleation rate line, $h0$. According to the nucleation theorem, the slope of the isothermal nucleation rate surface section in a log J vs log S space is determined by the new phase embryo size.[25] On a log J scale, this slope is infinitely large along the equilibrium line and the slope decreases to about unity along the spinodal decomposition line.

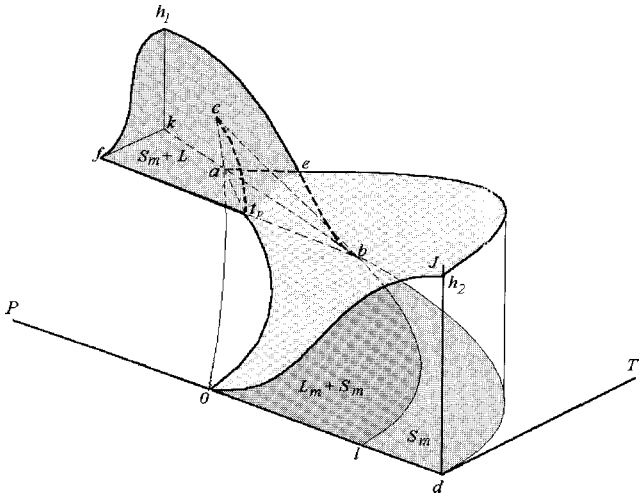

FIG. 3. A surface of a liquid cavitation (or boiling) rate, J (gray color) over the P-T phase diagram. The spinodal line cl (Ref. 20) is the projection of the highest nucleation rate line, hc. Line hc has a finite (nonzero) low temperature limit of nucleation rate and a zero nucleation rate at the critical point. The crystalline-vapor equilibrium is shown by the dotted line t_p0.

That is, the section slope must agree with the physical sense that critical embryo decrease in size from the infinitely large in the vicinity of the phase equilibrium to its smallest value at the spinodal decomposition conditions.

The nucleation rate in a superheated or cavitated crystalline state is shown in Fig. 4. A solid can be melted to the liquid phase or destroyed by tension. From formal considerations, the transition is to a region of an existing vapor (possibly condensed) or a transition to zero pressure in the absence of vapor (vacuum). The rate of nucleation is zero along the solid-liquid and solid-vapor lines of equilibrium. The S-L equilibrium line ends at the metastable triple point b where according to Rasmussen,[23] this line and both the crystalline state limit and cavitation spinodal lines intersect. At the critically unstable triple point, as at any spinodal line point, the vaporization phase transition has no activation barrier and zero enthalpy for the phase transition. The critically unstable triple point b is the end of the first order phase transition line (the solid-liquid equilibrium line). As a consequence, this point is the critical point for S-L equilibrium line.

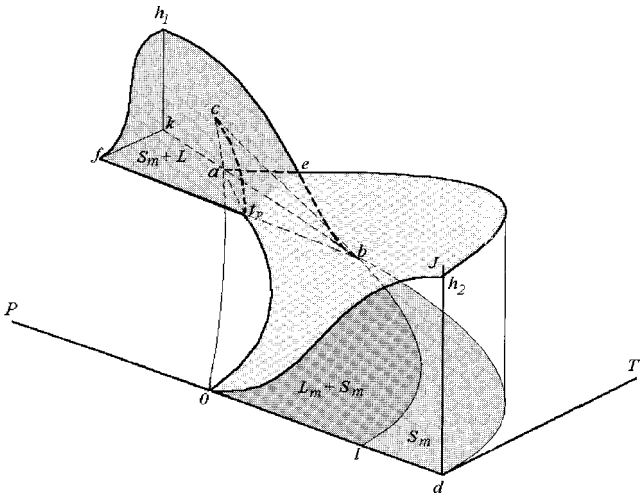

FIG. 4. The nucleation rate in a crystalline state. The surface of the liquid phase formation rate has a dark gray color of the contour ft_peh_1 and the invisible part ebt_p and the vapor embryo formation has a light gray color (contour $0h_2et_p$) and the hidden part eat_p.

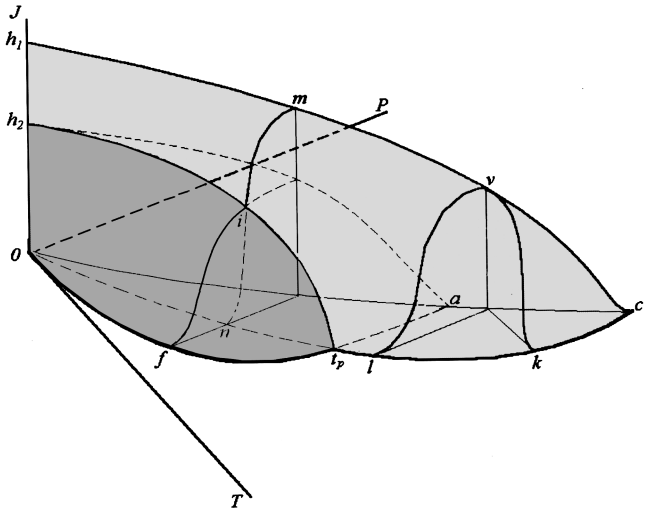

FIG. 5. The vapor nucleation rate surface. The surface of the nucleation rate of the liquid (or supercooled liquid) phase is drawn on the contour ct_pn0h_1m, light gray color, and of crystalline phase on the contour $0ft_pih_2$, dark gray color; the curve nim (or lv for liquid phase nucleation) and the curve fi for the crystalline phase are the rates of isothermal nucleation; curve vk is the nucleation rate at the constant pressure.

It is known that the S-L equilibrium has no high-pressure critical point at any achievable pressures. The nucleation rate line at high pressures can be such as the isobaric line fh_1 in Fig. 4. The line of highest nucleation rate h_1eb for the crystal transition to the liquid phase is above the spinodal line kab. The zero nucleation rate is at the critical point b fci S-L equilibrium. The surface of the liquid phase formation rate includes the dark gray colored contour ft_peh_1 and the invisible part ebt_p.

Strength theory[26] requires that crystalline states have a tension limit. This limit can be shown by the spinodal line abd (Fig. 4) for stretched crystal decomposition (or destruction). The resulting equilibrium line, $0t_pa$, is along a zero rate line for the solid-vapor transition. At the absolute zero

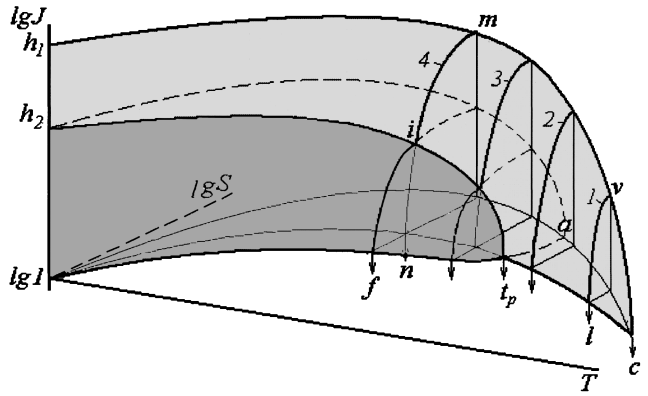

FIG. 6. The vapor nucleation rate surface in log(J)-log(S) space as it is in a regular experiment.

temperature limit, ideal crystals have their highest strength. The spinodal line for S-V transitions is a projection of the highest nucleation rate line aeh_2. The surface of the vapor embryo formation includes the light gray color (contour $0h_2et_p$) and the hidden part eat_p. Two surfaces on Fig. 4 must be in agreement with the strength theory in terms of the number of liquid or gaseous embryos per unit volume per unit time, as a function of the metastable state conditions. The vapor pressure in the critical embryos is always positive due to their high Laplace pressure although the crystal may be stretched in tension.

In Fig. 5, the vapor nucleation rate surface is shown. It can be seen that line $ca0$ is the projection of the highest nucleation rate line cmh_1. Line ct_pn0 representing the phase equilibrium is the zero rate boundary of the liquid nucleation rate surface. The surface of the nucleation rate of the liquid (or supercooled liquid) phase is drawn as the contour ct_pn0h_1m, the light gray color region in Fig. 5. The surface of the nucleation rate of crystalline phase covers the contour $0ft_pih_2$ (dark gray color in Fig. 5). At the low temperature limit, the metastable liquid and crystalline degrees of freedom are decreasing, and the accommodation probability of a single molecule on the cluster increases as the temperature decreases. These factors lead to a nonzero nucleation rate in the zero temperature limit. The nucleation rate in the low temperature limit is similar to the spinodal condition. Point 0 is a limit for the vapor spinodal lines. The condensed molecule mobility is reduced and therefore, the probability of obtaining the amorphous state is higher than the crystalline state and the nucleation rate for amorphous particles is higher.

To obtain the values of an isothermal rate of the liquid phase nucleation, the surface of the nucleation rate of the liquid (or metastable liquid) phase (Fig. 5) is bisected at a constant temperature. This process yields the curve nim (or lv) for liquid phase nucleation and curve fi for the rate of isothermal nucleation of the crystalline phase. An experimental rate of nucleation at the constant temperature is the sum of curves such as nm and fi. The isobaric rate of nucleation is obtained by cutting the surface at constant pressure (curve vk, Fig. 5).

Figure 5 can be converted to log-log space to yield log J against log S curves (Fig. 6) as are the typical formats in which experimental results are reported. The log J (log S, T) surface section projections at fixed temperatures are shown in Fig. 7. Equivalent curves have the same numeric labels in Figs. 6 and 7. The behavior of the nucleation rate curves as a function of vapor supersaturation (or activities) can be observed to be qualitatively correct.

The presence of a triple point produces nucleation rate isotherms with inflections (curves 3 and 4 in Figs. 6 and 7). The nucleation rate limit (shown by dotted curve mc in Fig. 7 as the projection of the line mvc in Fig. 6) can be found experimentally in a region of relatively high nucleation temperatures.

D. Nucleation rate surfaces for binary vapors

The rate surfaces for the nucleation of binary vapors are in a four-dimensional space, JTa_1a_2. At constant temperature, it possible to show the rates of nucleation of single vapors[11] (lines J_1 and J_2, Fig. 8). The nucleation rate curves of single vapors are connected by the nucleation rate surface of the two-component vapor. At a constant vapor activity, the nucleation rate curves 1 or 2 are obtained. With both species activities changing, curve 3 is obtained with projection 4. The vapor component solubility determines the form of the intersection line traced at a fixed rate of nucleation. This surface is the result of the qualitative examination of experimental studies for binary nucleation.[27]

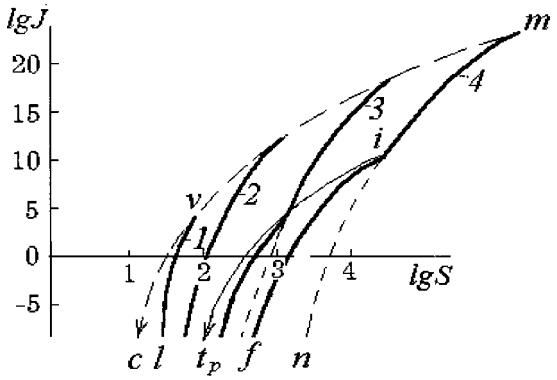

FIG. 7. Surface section projections (Fig. 6) at the fixed nucleation temperatures.

An ideal binary solution will provide the simplest P-X diagram with infinite solubility of components at a fixed temperature T, where P is the total system pressure and X is the composition of the binary solution. In this case, a cigarlike phase diagram is obtained (curves mfn and $nrgm$, Fig. 9).

The surface of the vapor nucleation rate can be drawn from the rates of nucleation of the individual components (curves nd and mh, Fig. 9). At the vapor equilibrium points (n,m), the rates of vapor nucleation are equal to zero. Nucleation rates have a maximum value over the spinodal points, h and d, for the single components. The points of maximum nucleation rates of the single components are connected by the line deh representing the maximum binary nucleation rates. In the simplest case, deh can be a straight line. The nucleation of a binary vapor with composition X_0 begins at point f, where point f is the first point of a pressure interval fg for the heterogeneous phase equilibrium at com-

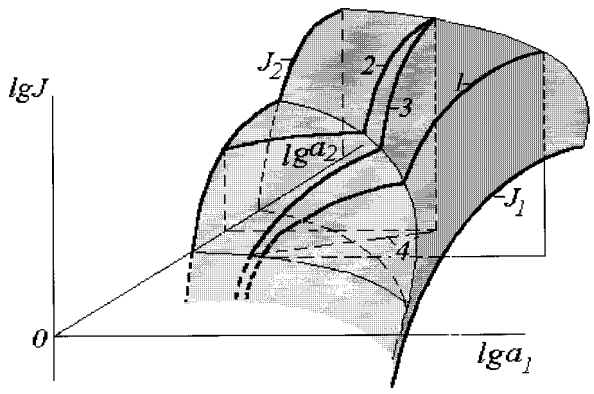

FIG. 8. Nucleation rate surface of the binary system log(J) vs the component vapor activities as log(a_1) and log(a_2).

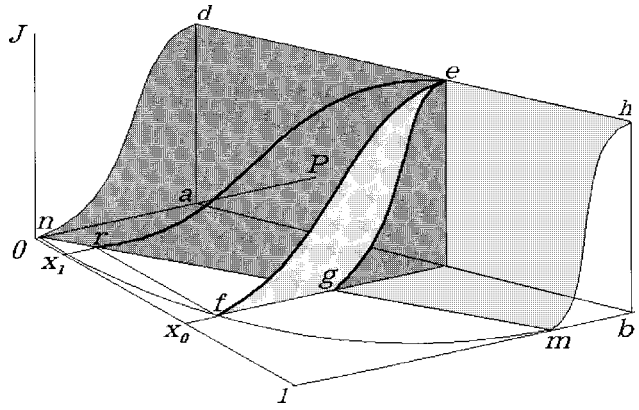

FIG. 9. Nucleation rate surface with known composition (dark gray color) of the new phase critical embryos for the binary ideal solution. X_0 and X_1 are compositions for the vapor and the critical embryo at zero nucleation rates, respectively; line fe is the projection of line re at X_0 diagram section (light gray).

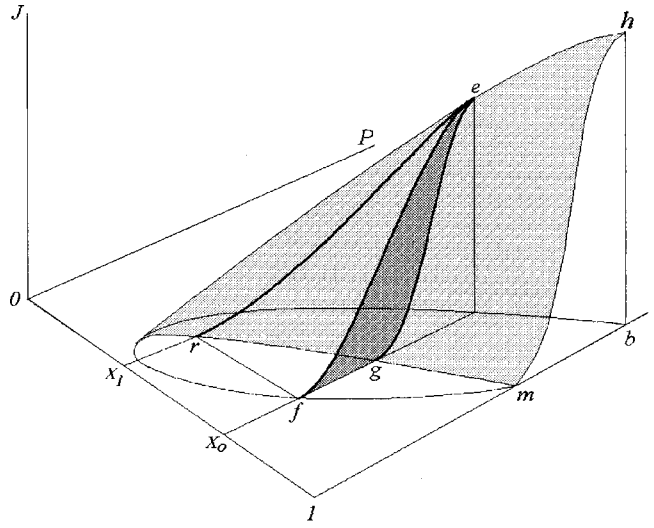

FIG. 10. Nucleation rate surface with known composition (gray color) of the new phase critical embryos for the binary ideal solution at the nucleation temperature between critical temperatures of pure components.

position X_0. The condensed phase has the composition X_1 at point r. For each point of line nfm, there is a corresponding point on line $nrgm$. Line $nrgm$ of the equilibria of the liquid and two-phase states is locus of points of zero nucleation rates and it must be the boundary of the nucleation rate surface.

The surface of the nucleation rate is represented by contour hednrgm. At the spinodal decomposition line, the compositions of the vapor and condensed phases coincide. An increase in pressure from point r to point e follows the rate line of vapor nucleation (re) at the fixed nucleation temperature T and with known composition of the critical embryos starting at the initial vapor composition X_0. Curve fe is the projection of the curve re on the state diagram at the composition X_0. In this case, the critical embryos have unknown compositions.

The presentation of the nucleation rate surface with unknown critical embryo composition is possible if all of the experimental vapor nucleation rates (such as the curve re) are attributed to the state diagram section (e.g., fe for the line re) at the point corresponding to the initial vapor composition (X_0). In this case, the zero rate points for vapor nucleation belong to the lower line of the cigarlike diagram. This surface has been drawn in the JXP space in Fig. 9. This surface can be converted to the space Ja_1a_2 previously shown in Fig. 8 and these figures show two alternative ways to present the rates of binary vapor nucleation.

The nucleation rate surface with unknown compositions of critical embryos is drawn on contour hednfm (Fig. 9) for an ideal binary solution. The equilibrium line between the gas and the heterogeneous phases gives zero rates of the vapor nucleation. It is the boundary of the nucleation rate surface for this case. It must be noted that the two methods of presenting the nucleation rate surface have quite different magnitude for vapor nucleation rates at the intermediate supersaturations. They cannot be defined at low rates along the unknown critical embryo composition surface whereas the surface of nucleation rate with known compositions of the critical embryos cannot be determined without specific structural models.

The phase diagram does not connect to the origin (Fig. 9) if the nucleation temperature T is between the critical temperatures of the two components (Fig. 10). There is then a lower composition boundary along the X axis for binary nucleation to occur. The top value (point h) of the nucleation rate of a component with a higher critical temperature is connected with the critical point at the temperature T by the line of maximum rates of a binary vapor nucleation. The rate of vapor nucleation at the critical point is equal to zero. The rest of the description of Fig. 10 is the same as for a cigarlike diagram (Fig. 9).

A binary system with partial solubility is presented in Fig. 11. It shows the nucleation rate surface for a binary system phase diagram with an eutectic point and partial solubility of the components. The nucleation rate surface of an analogous system with a peritectic point is shown in Fig. 12.

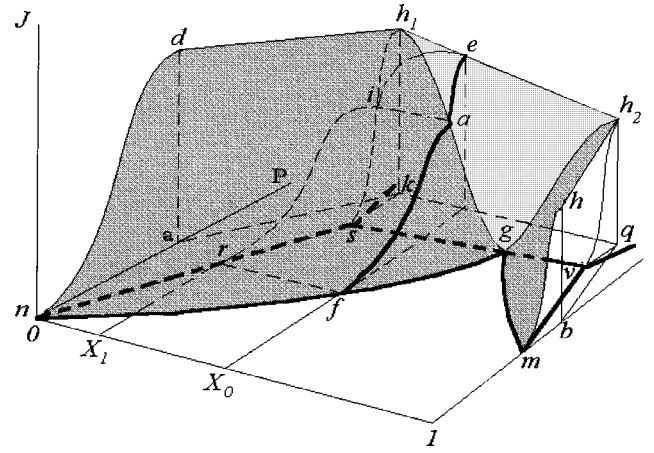

FIG. 11. Nucleation rate surface for the binary system phase diagram with eutectic point. A description for the cigarlike diagram given above is applicable for soluble compositions. Pressing the vapor with composition X_0 at a fixed temperature produces a new phase with composition X_1 at point f. The portion of low nucleation rate curve belongs to the solution surface until the composition reaches point s. Between point s and v, there are heterogeneous solutions with different ratios of the compositions X_s and X_v.

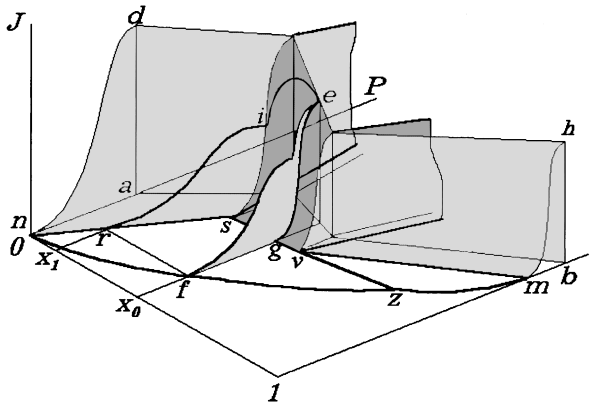

FIG. 12. Nucleation rate surface for the binary system phase diagram with peritectic point (see Fig. 11).

The description for the cigarlike diagram given for Fig. 9 is applicable for soluble composition portions of both Figs. 11 and 12. Nucleation of vapor with composition X_0 in the region of heterogeneous solutions will be discussed here with reference to both Figs. 11 and 12. Compressing vapor with composition X_0 at a fixed temperature produces a new phase with composition X_1 at point f. The portion ri of the low nucleation rate curve belongs to the homogeneous solution surface until the composition reaches point s. Between points s and v, there are heterogeneous solutions with different ratios of compositions X_s and X_v. The nucleation rate line ie corresponds to this interval. Line fae is the projection of the nucleation rate line rie (line rie provides known compositions of the new phase embryos) on the diagram at composition X_0. Line fae is part of the nucleation rate surface where the critical embryo compositions are unknown.

The sv interval of vapor compositions produces nucleation through two channels.[28] The rate of nucleation is the sum of rates of the bound points of soluble compositions. The vapor nucleation rate is determined by the relative contribution of the two vapor nucleation channels. The compositions of the critical embryos are X_s and X_v, respectively. In Fig. 13, the metastable region ($kqvs$) with the part of the nucleation rate surface has been drawn where the critical embryo compositions are known. If the vapor at initial composition X_0 is in the metastable state P_x (Fig. 13), the vapor nucleation rate, J_x, at this point can be expressed by summing the nucleation rates of the two channels for the given state P_x as

$$J_x L_{sv} = J_v L_{sx} + J_s L_{xv}, \tag{10}$$

where J_s and J_v are the nucleation rates through each of the two channels for the state P_x; $J_x = J_1 + J_2$; L_{sv}, L_{xv} and L_{sx} are the lengths of the line segments in Fig. 13, sv, sx, and xv, respectively. Equation (10) is similar to the lever rule in theoretical mechanics or in chemistry for heterogeneous phase equilibria. It can be generalized as a rule for nucleation: In binary systems with partial component solubility, there is a nucleation path with two channels[28] in the metastable state region ($sfgv$, Figs. 11 and 12). The particle number production rate for these channels obeys a lever rule for a vapor nucleation rate [such as Eq. (9)].

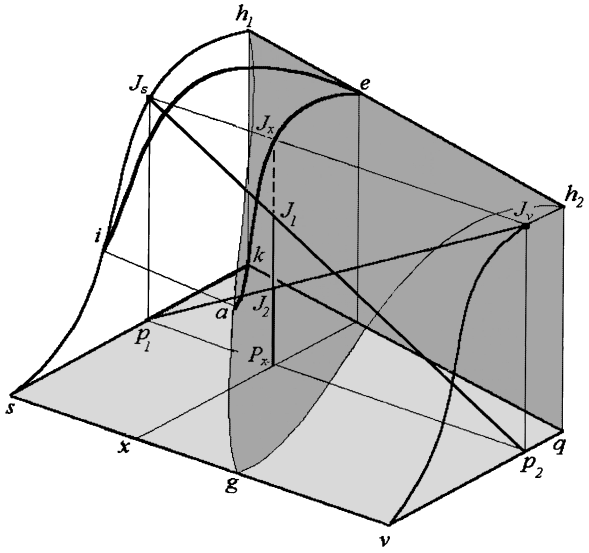

FIG. 13. Lever rule for nucleation rate.

At a fixed nucleation temperature higher than the critical point of a single component, the vapor compositions on the left-hand side of the critical point in Fig. 14 are of interest. A vapor which is compressed does not meet the phase equilibrium lines within this interval of parameters. Under supercritical conditions, there are homogeneous supercritical fluid states. Compression of the supercritical fluid under isothermal conditions eventually can produce nucleation of crystalline particles or condensation to a heterogeneous fluid. If the temperature is between critical temperatures of the mixture components, nucleation of a heterogeneous fluid can occur.

If a binary solution has a stable composition due a chemical reaction, or an interaction such as in the formation of a clathratelike structure, the phase diagram contains joint phase diagrams of two binary systems where this stable composition can be considered as the single substance and which provides the boundary for both individual binary diagrams. Figure 15 shows the surface of the nucleation rate of the system with a stable azeotrope composition X_s. Line am at constant vapor composition X_0 shows the isothermal nucleation rate with unknown critical embryo compositions. The

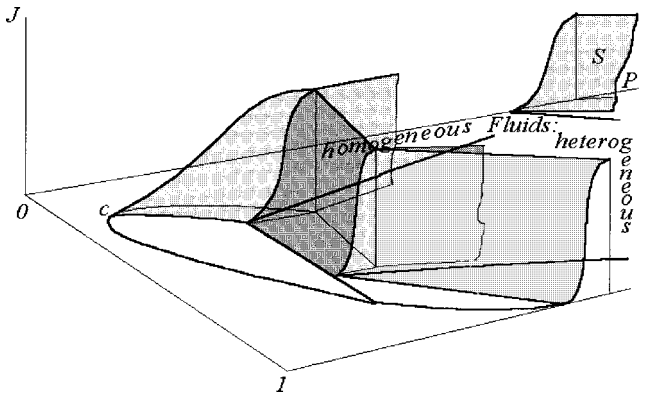

FIG. 14. Nucleation rate surface for the binary system phase diagram with peritectic point at the nucleation temperature between critical temperatures of pure components.

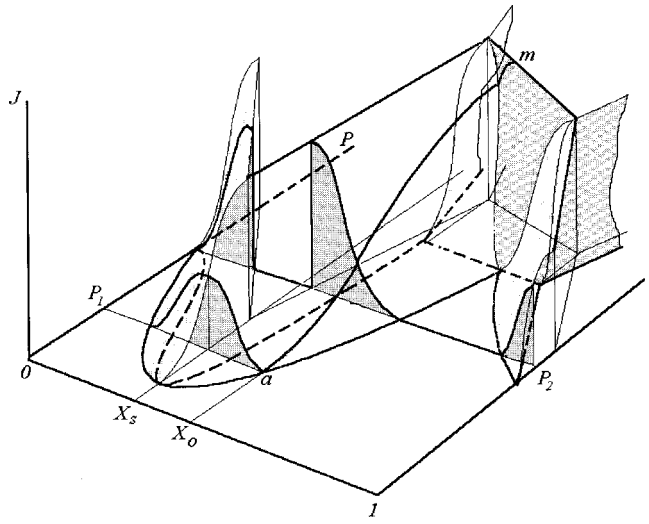

FIG. 15. Nucleation rate surface of the binary system with the stable azeotrope composition X_s. Line *am* at constant vapor composition X_0 shows the isothermal nucleation rate with unknown composition of the critical embryos. The section at the pressure P_1 can be considered to be retrograde condensation, where the boundaries of two nucleation rate surfaces coincide. The P_2 section produces trimodal nucleation rate curves.

nucleation rate surface section at pressures P_1 and P_2 shows an exotic behavior for the nucleation rates. The section at pressure P_1 can be considered to be retrograde condensation where the boundaries of two nucleation rate surfaces coincide. The P_2 section produces trimodal nucleation rate curves. This nucleation rate cannot be predicted by any nucleation theories. It would be useful to explore experimental measurement of these polymodal curves of the nucleation rate in the near future.

IV. DISCUSSION AND SUMMARY

The results above show that the nucleation rate surfaces develop from the phase diagram. Seemingly, using the relatively simple rules, a topology of the nucleation rates surfaces for each single or binary phase state diagram can be analyzed. The construction of the nucleation rate surfaces for ternary and higher dimensionality systems can be completed using computer simulation methods.

Scaling problems for the nucleation rate surface arise from the old problem of phase diagram scaling. It is well known that phase diagram scaling can only be done for some homologous series of chemical compounds. Thus, nucleation rate surfaces can be created for analogous homologous series. For the binary and higher dimensionality systems, nucleation rate scaling can be developed for systems with scaled phase diagrams.

Due the close connection of the phase state diagram with nucleation rates, it is not likely that nucleation rates can be predicted using only first principles because the temperatures of phase transitions are not currently predictable. A universal nucleation theory created on the basis of first principles is not available at the present. Partial theoretical success could be attained in the limited cases where there are well-known interaction potentials for a given species. Unfortunately, there is no universally applicable potential. Nucleation science suffers from the fundamental problem that an adequate description of the intermolecular interaction is not yet available. Progress in this area will improve nucleation theory.

Scaling of identical elements in the nucleation rate surfaces can be used to develop a nucleation rate topology for any phase state diagram. Scaling should give a quantitative scale for the nucleation rates. Phase diagrams must be taken into account in the interpretation of experimental nucleation results and further nucleation theory development.

ACKNOWLEDGMENTS

The work at Clarkson University was supported by U.S. National Research Council under a Cooperation in Applied Science and Technology (CAST) grant. In addition, Grant RFFR, No. 97-03-33586 to Kemerovo University is acknowledged for the partial support of the work there. The authors are grateful to Professor Howard Reiss for his support of the main ideas of this work and discussion of the nucleation rate topology of binary ideal solutions.

APPENDIX

Nomenclature

N	gas phase number densities
n	number of molecules in a cluster
$*$	sign for parameters of a critical embryo
β_i	impinging frequency of molecules with i-size cluster
t	time
$C(n)$	actual concentration of n-size clusters
$c(n,t)$	equilibrium concentration of n-size clusters
t_p	triple point
J	number of clusters changed from n to $n+1$ size per unit of time in the unit of volume
$\square G$	Gibbs free energy of a single cluster;
T	temperature
P	total pressure
k	the Boltzmann constant
Z	the Zeldovich nonequilibrium factor
B	kinetic factor
C (or c)	critical point
v_1	volumes per molecule in a liquid phase
$S=p_v/p_s$	vapor supersaturation ratio
p_v	actual vapor pressure
p_s	equilibrium vapor pressure
r	cluster radius
σ	surface tension
μ	chemical potential
Δ	the width of the saddle point
a_i	chemical activity of the i-th species
s_1	spinodal line
X	composition of a binary solution

Phase states

L	liquid
S	solid
V	vapor
m	subscript, denotes a metastable state

[1] C. T. R. Wilson, Philos. Trans. R. Soc. London, Ser. A **189**, 265 (1897).
[2] D. W. Gibbs, *Elementary Principles in Statistical Mechanics: Developed with Especial Reference to the Rational Foundation of Thermodynamics* (Ox Bow, Woodbridge, 1981).
[3] L. Farkas, Z. Phys. Chem., Stoechiom. Verwandtschaftsl. **125**, 236 (1927).
[4] R. Becker and W. Doring, Ann. Phys. (Paris) **24**, 719 (1935).
[5] M. Volmer and A. Weber, Z. Phys. Chem., Stoechiom. Verwandtschaftsl. **19**, 277 (1926).
[6] H. Flood, Z. Phys. Chem. Abt. A **170**, 186 (1934).
[7] J. Frenkel, *Kinetic Theory of Liquids* (Oxford University Press, London, 1946).
[8] J. B. Zeldovich, Acta Physicochim. USSR **18**, 1 (1943); J. B. Zeldovich, Zh. Exp. Theor. Phys. (USSR) **12**, 525 (1942).
[9] H. Reiss, J. Chem. Phys. **18**, 840 (1950).
[10] M. P. Anisimov, J. Aerosol Sci. **21**, 23 (1990).
[11] M. P. Anisimov and K. M. Anisimov, Abstracts, Fourth International Aerosol Conference, 1994, edited by R. C. Flagan (unpublished), Vol. 1, p. 109.
[12] V. A. Shneidman, Zh. Techn. Phys. (Russian) **57**, 131 (1987).
[13] T. Hill, J. Chem. Phys. **36**, 3183 (1962); *Thermodynamics of Small Systems. Part I and Part II*. (Benjamin, New York, 1964).
[14] S. Girshick and C.-P. Chiu, J. Chem. Phys. **93**, 1273 (1990); S. Girshick, C.-P. Chiu, and P. McMurry, Annu. Rev. Earth Planet Sci. **13**, 465 (1990); S. Girshick, J. Chem. Phys. **94**, 826 (1991).
[15] A. Dilman and G. Meier, Chem. Phys. Lett. **160**, 71 (1989); J. Chem. Phys. **94**, 3872 (1991).
[16] D. Stauffer, J. Aerosol Sci. **7**, 319 (1976).
[17] P. Mirabel and J. L. Katz, J. Chem. Phys. **60**, 1138 (1974).
[18] J. L. Kassner and R. J. Schmitt, J. Chem. Phys. **44**, 4166 (1966).
[19] D. W. Oxtoby, J. Phys.: Condens. Matter **4**, 7627 (1992).
[20] V. P. Skripov and M. Z. Faizulin, High Temp.-High Press. **18**, 1 (1986).
[21] P. G. Debenedetti, *Physical Chemistry of Aqueous Systems*, edited by H. J. White, Jr., J. V. Sengers, D. B. Neuron, and J. C. Bellows (Wallingford, New York, 1995), p. 339; P. G. Debenedetti and M. C. D'Antonio, AIChE. J. **34**, 447 (1988).
[22] V. P. Skripov and V. G. Baidakov, Teplofiz. Vys. Temp. **10**, 1226 (1972).
[23] D. H. Rasmussen and M.-T. Liang, *Proceedings of the Symposium on Nucleation and Crystallization in Glasses and Liquids, Atlanta, 1985* (American Ceramic Society, 1993).
[24] R. J. Speedy, J. Phys. Chem. **86**, 982 (1982).
[25] M. P. Anisimov and A. G. Cherevko, Izv. Akad. Nauk USSR (Siberian Branch) (ser.KhNauk) **2**, 15 (1982); D. Kashchiev, J. Chem. Phys. **76**, 5098 (1982).
[26] R. Houwink, *Elasticity, Plasticity and Structure of Matter* (Harren, Washington, DC, 1953).
[27] M. P. Anisimov, S. N. Vershinin, A. A. Akseniov, A. M. Sgonnov, and G. L. Semin, Kolloidn. Zh. **49**, 842 (1987); R. Strey and P. E. Wagner, J. Aerosol Sci. **19**, 813 (1988).
[28] A. K. Ray, M. Chalam, and L. K. Peters, J. Chem. Phys. **85**, 2161 (1986).